Table 1. Frequencies of p16 HDs and EGFR/KRAS/p53 mutations in lung adenocarcinoma

Sample	Subtype	Frequency (%)			
		p16	EGFR	KRAS	p53
Surgical specimen		13/50 (26)	34/50 (68)	4/50 (8)	32/50 (64)
Primary tumor		8/28 (29)	21/28 (75)	2/28 (7)	16/28 (57)
	Type B	2/8 (25)	8/8 (100)	0/8 (0)	2/8 (25)
	Type C	4/15 (27)	12/15 (80)	1/15 (7)	9/15 (60)
	Type D	2/5 (40)	1/5 (20)	1/5 (20)	5/5 (100)
Brain metastasis		5/22 (23)	13/22 (59)	2/22 (9)	16/22 (73)
Cell line*		20/55 (36)	-	-	-

*Defined in our previous study (17).

previously examined for mutations of exons 18 to 21 in the *EGFR* gene, of exons 1 and 2 in the *KRAS* gene, and of exons 4 to 8 in the *p53* gene by genomic PCR and direct sequencing (14, 16). The remaining 15 primary tumors and 6 brain metastases were also examined for these mutations in this study using the same methods.

Statistical analysis. Fisher's exact test was used to assess the association of p16 HDs with clinicopathologic characteristics or mutations of the *EGFR*, *KRAS*, and *p53* genes. $P < 0.05$ was considered to be statistically significant.

Results and Discussion

Detection of HDs by MLPA analysis. We previously determined regions of p16 HDs in various lung cancer cell lines by multiplex genomic PCR analysis (3, 17). Thus, we first validated the sensitivity and specificity of the MLPA method to detect p16 HDs using several lung adenocarcinoma cell lines. No PCR amplification was observed for probes that hybridized to the sequences of HD regions in all the cell lines examined. Representative results of MLPA analysis for two cell lines, H2126 and PC3, are shown in Fig. 1B. We then applied MLPA analysis for the detection of p16 HDs in surgically resected adenocarcinoma samples. Cancer cells of small-sized primary adenocarcinomas were isolated by laser capture microdissection, and brain metastases generally contain a small fraction of noncancerous cells. However, a complete absence of PCR products was not observed for these samples at any chromosomal loci by MLPA analysis. Therefore, we next defined the criteria for p16 HDs by MLPA analysis for surgically resected samples. For this purpose, DNA samples with virtual hemizygous deletions were prepared by mixing the same amounts of DNA from normal lung tissue and from three lung cancer cell lines with p16 HDs, H2126, A549, and PC3. In total, 64 probe loci were homozygously deleted in these cell lines. The mean ± 3 SD of relative DNA copy number ratios for the 64 probe loci in the HD regions among these mixed samples was 0.54 ± 0.17; thus, the range of virtual hemizygous deletions was 0.37 to 0.71. Indeed, none of the 64 probe loci in the HD regions of the mixed samples showed a DNA copy number ratio of >0.71 or <0.37 (Fig. 1B). Therefore, if the DNA copy number ratio for a locus was <0.37, the locus was judged as homozygously deleted in surgically resected lung adenocarcinoma samples.

Under this criterion, one or more loci in the *p15/p14ARF/p16* gene region were judged as homozygously deleted in 8 of 28 primary tumors and in 5 of 22 brain metastases (Table 1). Representative adenocarcinoma cases judged as having HDs of this region by MLPA analysis are shown in Fig. 1C. Case B-2P showed a HD of only one locus (probe no. 13) in exon 2 of the *p16* gene. On the other hand, most of the other 12 cases showed HDs of several genes, including the *p14ARF* and/or *p16* genes (Table 2). Both the invasive region (C-10P-in) and the BAC component (C-10P-BAC) of case C-10P showed HDs of the same loci from *p15* exon 1 to *IFNW1*. In case D-4P, the *p15*, *p14ARF*, *p16*, and *MTAP* genes were homozygously deleted. A metastasis to the brain, case N2131M, showed a large HD of the region from the *ELAVL2* gene to the *IFNB1* gene including the *p16* gene. Furthermore, the relative DNA copy number ratios of the corresponding loci were also decreased in the corresponding primary tumor, N2133P, although the ratios were underrepresented as HDs. This may be attributed to a

Table 2. Regions of p16 HDs on chromosome 9p defined by MLPA analysis

No.	Case		Probe no.																							
	Primary tumor	Brain metastasis	1	2	3	4	5	6	7	8	9	10	11	12	13	14	15	16	17	18	19	20	21	22	23	24
1	B-2P		-	-	-	-	-	-	-	-	-	-	-	-	+	-	-	-	-	-	-	-	-	-	-	-
2	B-8P		-	+	-	+	+	+	-	+	+	-	+	+	+	+	+	+	-	-	-	-	-	-	-	-
3	C-5P		-	-	+	+	+	+	+	+	+	+	+	+	+	+	+	+	+	+	+	+	+	+	+	-
4	C-8P		-	+	+	+	+	+	+	+	+	+	+	+	+	+	+	+	+	+	+	+	+	+	+	-
5	C-10P		-	-	+	+	+	+	+	+	+	+	+	+	+	+	+	+	+	+	+	+	-	-	-	-
6	C-65P		-	-	+	+	+	+	+	+	+	-	+	+	+	+	+	+	+	+	+	-	-	-	-	-
7	D-4P		-	-	+	+	+	+	+	+	+	+	+	+	+	+	+	+	-	-	-	-	-	-	-	-
8	D-12P		-	+	+	+	+	+	+	+	+	+	+	+	+	+	+	+	+	+	+	+	+	-	-	-
9		N181M	-	-	+	+	+	+	+	+	+	+	+	+	+	+	+	+	-	-	-	-	-	-	-	-
10		N571M	-	-	+	+	+	+	+	+	+	+	+	+	+	+	+	+	-	-	-	-	-	-	-	-
11	N2133P	N2131M	-	+	+	+	+	+	+	+	+	+	+	+	+	+	+	+	+	+	+	+	+	-	-	-
12		N2151M	-	-	+	+	+	+	+	+	+	+	+	+	+	+	+	+	+	+	+	+	+	+	-	-
13		N2191M	-	+	+	+	+	+	+	+	-	-	-	-	-	-	-	-	-	-	-	-	-	-	-	-

NOTE: Loci with copy number ratios <0.37 are indicated by (+) and those >0.37 are indicated by (-).

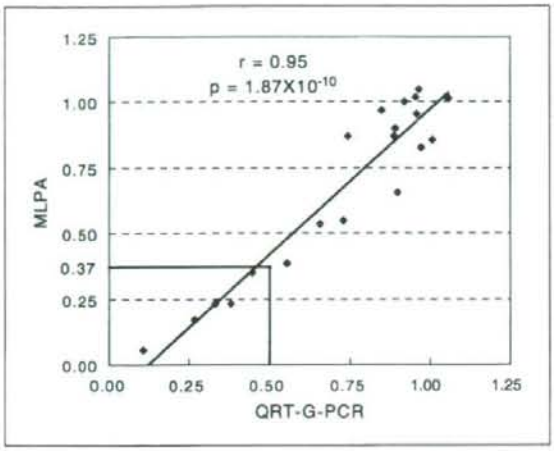

Fig. 2. Correlation between the results of MLPA analysis and those of QRT-G-PCR analysis. Relative DNA copy numbers of the probe no. 9 locus in Fig. 1A on chromosome 9 against the control locus on chromosome 2 defined by the QRT-G-PCR (*X*-axis) and MLPA analyses (*Y*-axis). Sixteen brain metastases and four of the corresponding primary tumors were analyzed. Values <0.5 by QRT-G-PCR analysis and values <0.37 by MLPA analysis (indicated by lines) were considered as having HDs.

contamination of noncancerous cells in the primary tumor sample because this sample was macrodissected but not microdissected. There was no probe loci deleted in all the cases, but six loci (probe nos. 4, 5, 6, 8, 9, and 13) were deleted in 12 of 13 cases, including exon 2 of the *p16* gene (Table 2).

Confirmation of HDs by QRT-G-PCR analysis. QRT-G-PCR was performed to confirm p16 HDs detected by MLPA analysis. Among 15 control probes for nonchromosome 9p loci, a probe for a chromosome 2p14 locus showed the most consistent DNA copy number ratios of nearly 1.0 in surgically resected adenocarcinoma samples. Thus, two primer sets were designed for QRT-G-PCR analysis. One was for the amplification of an MLPA probe locus between the *p14ARF* gene and the *p16* gene (probe no. 9 in Fig. 1A, and hereinafter referred to as the *p14ARF/p16* locus), and the other was for the amplification of a control probe locus on chromosome 2p14.

QRT-G-PCR was carried out for 16 brain metastases and the corresponding 4 primary tumors. Among them, five brain metastases were judged as having HDs of the *p14ARF/p16* locus by MLPA analysis. DNA from normal lung tissue was used as a negative control, and DNA from two lung cancer cell lines with p16 HDs, A549 and H2126, were used as positive controls. No PCR products were detected for the *p14ARF/p16* locus in the A549 and H2126 cell lines (data not shown). The DNA copy number ratios of the *p14ARF/p16* locus in all five cases that had been determined to have HDs of this locus by MLPA analysis were <0.45. Thus, these five cases were also judged as having less than one copy of the *p14ARF/p16* gene by QRT-G-PCR analysis. We further analyzed the association between the results of MLPA analysis and those of QRT-G-PCR analysis among all the 20 cases. The correlation coefficient was 0.95, and a highly significant correlation was observed between them ($P = 1.87 \times 10^{-10}$; Fig. 2). This result gave the agreement for the appropriateness of the criterion for p16 HDs in MLPA analysis.

Occurrence of p16 HDs in early stage lung adenocarcinoma. Based on the results of MLPA analysis, together with the confirmation by QRT-G-PCR analysis, we concluded that p16 HDs were present in 8 of 28 (29%) small-sized primary tumors and in 5 of 22 (23%) brain metastases (Table 1). Among four pairs of brain metastases and the corresponding primary tumors, only one metastasis (N2131M) was judged as having a p16 HD as described above and shown in Fig. 1C, and none of the remaining three cases showed HD in either brain metastases or primary tumors. Small-sized adenocarcinomas

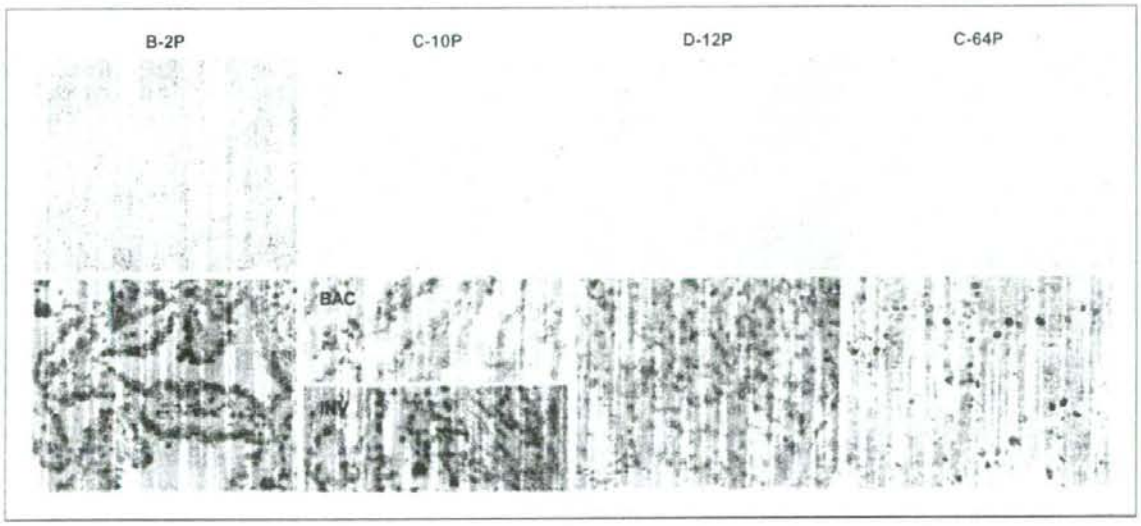

Fig. 3. Histology (H&E; original magnification, ×100 for B-2P/C-12P/C-64P and ×40 for C-10P; *top*) of small-sized lung adenocarcinomas and immunohistochemical staining of p16 protein (original magnification, ×400; *bottom*) in the corresponding tissues. B-2P, C-10P, and D-12P are representative cases of type B, C, and D tumors with p16-negative staining, and C-64P is a representative case of type C tumors with p16-positive staining. A BAC component (*BAC*) and an invasive region (*INV*) are shown separately for C-10P.

Table 3. Associations of p16 HDs with p16 protein expression, clinicopathologic characteristics, and EGFR/KRAS/p53 mutations in lung adenocarcinoma

Clinicopathologic characteristic and genotype	Subset	No. of cases	p16 HD (%)				P*
			+	-			
p16 protein expression †	+	13	0 (0)	13 (100)			<0.01
	-	15	8 (53)	7 (47)			
Gender	Male	30	7 (23)	23 (77)			0.74
	Female	20	6 (30)	14 (70)			
Age	<59	25	8 (32)	17 (68)			0.52
	≥59	25	5 (20)	20 (80)			
Smoking history	Smoker	28	7 (25)	21 (75)			>0.99
	Nonsmoker	22	6 (27)	16 (73)			
Pathologic stage †	I	16	5 (31)	11 (69)			>0.99
	II-III	12	3 (25)	9 (75)			
5-year survival †	+	19	4 (21)	15 (79)			0.37
	-	9	4 (44)	5 (56)			
EGFR/KRAS ‡	E(+)/K(-)	34	10 (29)	24 (71)	]>0.99		
	E(-)/K(+)	4	1 (25)	3 (75)		]>0.99	0.47
	E(-)/K(-)	12	2 (17)	10 (83)			
p53	Mutation(+)	32	9 (28)	23 (72)			0.75
	Mutation(-)	18	4 (22)	14 (78)			

*Fisher's exact test.
† Defined for 28 patients with primary lung adenocarcinoma.
‡ E(+), EGFR mutation(+); E(-), EGFR mutation(-); K(+), KRAS mutation(+); K(-), KRAS mutation(-).

were further classified histologically into types B, C, and D (Fig. 3). Type B tumors are noninvasive BACs and type C tumors are invasive adenocarcinomas with noninvasive BAC components. p16 HDs were detected in 2 of 8 (25%) type B tumors and in 4 of 15 (27%) type C tumors, in particular, in BAC components of two type C tumors (cases C-10P and C-65P). Type D tumors are invasive, poorly differentiated adenocarcinomas and p16 HDs were detected in 2 of 5 (40%) of the type D tumors. Thus, p16 HDs were present with similar frequencies of 25% to 40% in noninvasive and invasive primary adenocarcinomas. We previously reported that p16 HDs were present in 20 of 55 (36%) lung adenocarcinoma cell lines (17). Thus, the frequency of p16 HDs in small-sized primary adenocarcinomas was not significantly lower than, but similar to, those in brain metastases and cultured cell lines. These results strongly indicate that most p16 HDs detected in the cell lines occurred *in vivo* during adenocarcinoma progression and were retained during cultivation *in vitro* of adenocarcinoma cell lines. Similar frequencies of p16 HDs between noninvasive and invasive adenocarcinomas and between primary and metastatic adenocarcinomas further indicate that p16 HD occurs early in the multistage carcinogenic process of lung adenocarcinomas.

No p16 expression in tumors with p16 HDs. Because one of the purposes of this study was to confirm the immunohistochemical negativity of adenocarcinoma cells with p16 HDs, we further performed an immunohistochemical analysis on 28 cases of small-sized adenocarcinomas, all of which were subjected to MLPA analysis. Fifteen of the 28 cases (54%) showed negative immunoreactivity for p16 protein. As predicted, all eight cases with p16 HDs following MLPA analysis were negative for p16 protein expression (Table 3). Representative results of immunohistochemical staining for type B, C, and D tumors are shown in Fig. 3. It was noted that most tumor cells were clearly negative for nuclear p16 staining in these eight cases, and that both BAC components and invasive regions were negative in all four type C tumors with p16 HDs. This result strongly supports the reliability of MLPA analysis for the detection of p16 HDs in primary lung adenocarcinomas. Thus, it was concluded that p16 protein is not expressed in a considerable fraction of small-sized lung adenocarcinomas due to HDs of the p16 gene. The consistency of the results of immunohistochemistry with that of MLPA analysis further supports the hypothesis that *p16* HD occurs early in lung adenocarcinoma progression.

Previously, Dr. Noguchi, who is one of the authors of this article, and his colleagues reported that 29 of 57 (51%) small-sized lung adenocarcinomas of types A to F were negative for p16 immunostaining (7). In their report, the frequency of p16 negativity was higher in smokers and in patients with non-BACs. Aberrant methylation of the *p16* gene promoter was detected more frequently in advanced BACs (type C) and non-BAC (types D–F) than in BACs (types A and B). In this study, the overall frequency (54%) of p16 negativity was quite similar to their reports, and the frequency was also higher in smokers than in nonsmokers (9 of 13 versus 6 of 15), and in type D (5 of 5) than in type B (7 of 15) or type C (3 of 8). Thus, it was highly suggested that a majority of cases with negative p16 expression without p16 HDs could be due to methylation of the *p16* gene promoter and the methylation was associated with tobacco smoking. However, methylation and HD are not likely to coexist with each other because the regions of HDs in most of the 13 cases with HDs included the promoter region of the *p16* gene (from probe no. 8 to probe no. 11). Thus, either methylation or HD of the *p16* gene was suggested to occur equally and independently in smokers, whereas HD dominates in nonsmokers.

Association of p16 HDs with clinicopathologic characteristics. We then investigated the association of p16 HDs with clinicopathologic characteristics, including smoking history, of

patients with lung adenocarcinomas (Table 3). No significant associations were observed between p16 HDs and gender, age, and smoking history in all 50 cases analyzed (Table 3), as well as in 28 cases of primary adenocarcinomas or in 22 cases of brain metastases (data not shown). p16 HDs were not associated with pathologic stage nor with 5-year survival in 28 cases of primary adenocarcinomas (Table 3). Previously, p16 methylation was shown to be associated with smoking history (1, 7). Thus, no association of p16 HDs with smoking history was in contrast with the status of p16 methylation in lung adenocarcinomas. The results indicate that causative factors for p16 HD were different from those for p16 methylation, although both alterations result in the inactivation of the same gene. Previously, Kraunz and colleagues reported that p16 HD occurred at a higher frequency in never-smokers as compared with former and current smokers (6). Although such an association was not observed in this study, both studies indicated the absence of a positive association between p16 HD and smoking history, and the possible association of p16 HD with other causative factors for lung adenocarcinoma. Thus, further studies are needed for the elucidation of such factors because little is known about the environmental as well as genetic risk factors for lung adenocarcinoma. The absence of any association between p16 HDs and 5-year survival was also in contrast with the status of p16 methylation in lung adenocarcinomas. However, because the number of cases examined was small (28 cases), and the patients with poor prognosis had a higher frequency of p16 HDs than those with good prognosis (44% versus 21%), further studies will be required on this subject. The absence of any association between p16 HDs and pathologic stage further supports their occurrence in the early stages, rather than in the late stages, of lung adenocarcinoma progression.

Association of p16 HDs with EGFR, KRAS, and p53 mutations. We next evaluated the association of p16 HDs with the status of EGFR, KRAS, and p53 mutations in these samples (Tables 1 and 3). Then, based on the results of these molecular analyses and a previous p16 methylation analysis (7), a stepwise malignant progression model for small-sized lung adenocarcinoma was depicted as shown in Fig. 4. As previously reported (14, 18), EGFR and KRAS mutations were detected in a mutually exclusive manner in lung adenocarcinomas. EGFR mutations were most frequently detected in type B tumors (8 of 8, 100%), suggesting the involvement of EGFR mutations in the formation of noninvasive BACs. Although KRAS mutations were detected only in type C and D tumors in this study, it was recently reported that the mutations were frequently detected in noninvasive adenocarcinomas and also in atypical adenomatous hyperplasias (AAH; ref. 19). Thus, it is likely that either EGFR or KRAS mutations occur prior to HDs and methylations of the p16 gene in the progression of BACs, although it is also possible that p16 alterations occur earlier than depicted in Fig. 4. Frequencies of p53 mutations in primary adenocarcinomas were the highest in type D (5 of 5, 100%), intermediate in type C (9 of 15, 60%), and the lowest in type B (2 of 8, 25%), suggesting the accumulation of the mutations during progression from noninvasive adenocarcinomas to invasive ones. Thus, it was likely that p53 mutations had accumulated in adenocarcinomas with p16 HDs and/or EGFR/KRAS mutations. It is indispensable to analyze a considerable number of AAHs as well as type A tumors to fully understand the timing of each genetic alteration in sequential progression of lung adenocarcinomas because AAH is a putative precursor of peripheral lung adenocarcinoma including BAC (20), and sequential progression from type A to type C tumors through type B tumors was strongly indicated in previous

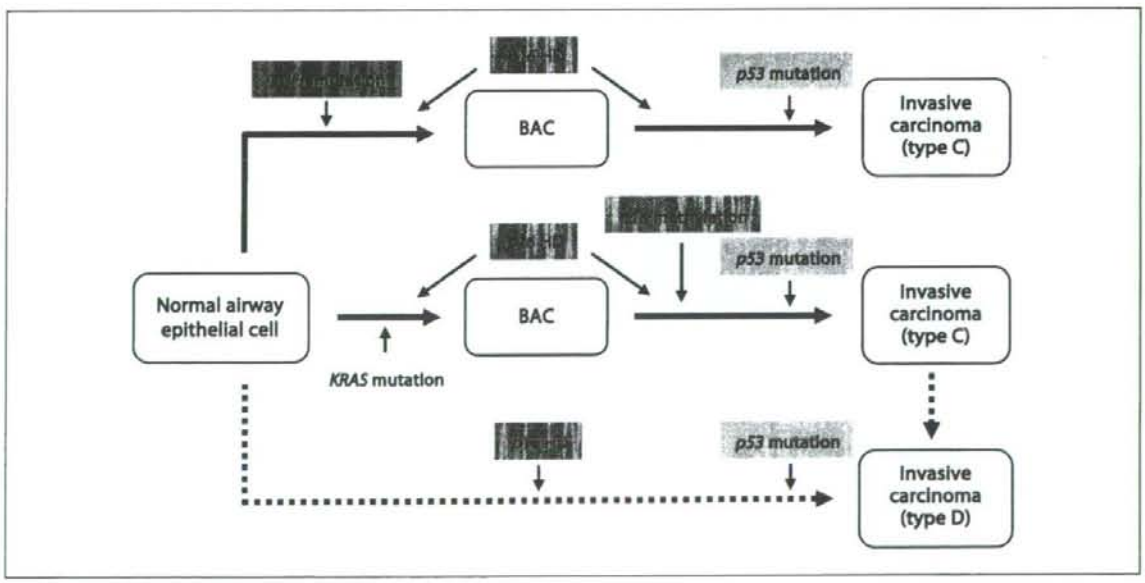

Fig. 4. A stepwise malignant progression model of small-sized lung adenocarcinoma in association with accumulated genetic alterations in cells. BAC, bronchioloalveolar carcinoma; type C, localized bronchioloalveolar carcinoma with foci of active fibroblastic proliferation; type D, poorly differentiated adenocarcinoma.

studies (7, 21). However, because AAH is not routinely resected by surgery and because type A tumors are usually very small, the number of tumors as well as the amount of DNA obtained was not enough for the present study.

There was no specificity for the occurrence of p16 HDs among adenocarcinomas with regard to other accompanied genetic alterations. In particular, p16 HDs were detected with similar frequencies (17–29%), irrespective of the presence or absence of EGFR, KRAS, and p53 mutations (Table 3). This result indicates that p16 HDs occur with similar frequencies in EGFR type as well as KRAS type and non-EGFR/KRAS type adenocarcinomas. In this model, type C tumors were considered to progress from BACs, as previously indicated by Aoyagi and colleagues (21). However, it was still unclear whether type D tumors arise *de novo* by a distinct pathway from tumors with BAC components or progress from these tumors. Low frequencies of EGFR mutations and high frequencies of p53 mutations in type D tumors indicate that type D tumors progress from either the KRAS types or non-EGFR/KRAS types. Haneda and colleagues also reported a low frequency of EGFR mutations in type D tumors (22), supporting the presence of a non-EGFR pathway for the development of type D poorly differentiated adenocarcinomas.

Conclusions. MLPA analysis of microdissected small-sized primary adenocarcinoma cells revealed that p16 HDs are present in 20% to 40% of adenocarcinomas irrespective of the presence of mutations in the *EGFR*, *KRAS*, and *p53* genes, and occur early in the development of lung adenocarcinomas. HDs were not associated with smoking history of the patients. It has been indicated that smoking is a major factor inducing p16 methylation as well as KRAS mutation. In contrast, EGFR mutations frequently occur in female nonsmokers and are associated with bronchioloalveolar morphology of adenocarcinomas. Interestingly, p16 HDs did not coexist with specific genetic alterations in adenocarcinoma cells. Thus, causative factors for p16 HD would be different from those for p16 methylation, KRAS mutations, and EGFR mutations. To elucidate the causative role for the occurrence of p16 HDs in multistage lung carcinogenesis, further studies should focus on the identification of environmental and genetic factors for the induction of DNA double-strand breaks surrounding the *p16* gene locus and their repair systems.

Disclosure of Potential Conflicts of Interest

No potential conflicts of interest were disclosed.

Acknowledgments

We thank Drs. Higashi and Yokoyama of FALCO Biosystems, Ltd., for their technical support and critical discussion in MLPA analysis. We also thank Drs. Nakanishi and Matsumoto for the laser capture microdissection of cancer cells from primary small-sized lung adenocarcinomas.

References

1. Toyooka S, Tokumo M, Shigematsu H, et al. Mutational and epigenetic evidence for independent pathways for lung adenocarcinomas arising in smokers and never smokers. Cancer Res 2006;66:1371–5.
2. Sato M, Shames DS, Gazdar AF, Minna JD. A translational view of the molecular pathogenesis of lung cancer. J Thorac Oncol 2007;2:327–43.
3. Hamada K, Kohno T, Kawanishi M, Ohwada S, Yokota J. Association of CDKN2A(p16)/CDKN2B(p15) alterations and homozygous chromosome arm 9p deletions in human lung carcinoma. Genes Chromosomes Cancer 1998;22:232–40.
4. Sanchez-Cespedes M, Reed AL, Buta M, et al. Inactivation of the INK4A/ARF locus frequently coexists with TP53 mutations in non-small cell lung cancer. Oncogene 1999;18:5843–9.
5. Sanchez-Cespedes M, Decker PA, Doffek KM, et al. Increased loss of chromosome 9p21 but not p16 inactivation in primary non-small cell lung cancer from smokers. Cancer Res 2001;61:2092–6.
6. Kraunz KS, Nelson HH, Lemos M, Godleski JJ, Wiencke JK, Kelsey KT. Homozygous deletion of p16INK4a and tobacco carcinogen exposure in non-small cell lung cancer. Int J Cancer 2006;118:1364–9.
7. Tanaka R, Wang D, Morishita Y, et al. Loss of function of p16 gene and prognosis of pulmonary adenocarcinoma. Cancer 2005;103:608–15.
8. Chen JT, Chen YC, Wang YC, Tseng RC, Chen CY, Wang YC. Alterations of the p16(ink4a) gene in resected nonsmall cell lung tumors and exfoliated cells within sputum. Int J Cancer 2002;98:724–31.
9. Schouten JP, McElgunn CJ, Waaijer R, Zwijnenburg D, Diepvens F, Pals G. Relative quantification of 40 nucleic acid sequences by multiplex ligation-dependent probe amplification. Nucleic Acids Res 2002;30:e57.
10. Worsham MJ, Chen KM, Tiwari N, et al. Fine-mapping loss of gene architecture at the CDKN2B (p15INK4b), CDKN2A (p14ARF, p16INK4a), and MTAP genes in head and neck squamous cell carcinoma. Arch Otolaryngol Head Neck Surg 2006;132:409–15.
11. Mistry SH, Taylor C, Randerson-Moor JA, et al. Prevalence of 9p21 deletions in UK melanoma families. Genes Chromosomes Cancer 2005;44:292–300.
12. Sobin LH, Wittekind CH, editors. TNM classification of malignant tumours. 6th ed. New York: Wiley-Liss; 2002. p. 99–103.
13. Noguchi M, Morikawa A, Kawasaki M, et al. Small adenocarcinoma of the lung. Histologic characteristics and prognosis. Cancer 1995;75:2844–52.
14. Matsumoto S, Iwakawa R, Kohno T, et al. Frequent EGFR mutations in noninvasive bronchioloalveolar carcinoma. Int J Cancer 2006;118:2498–504.
15. Sakamoto H, Mori M, Taira M, et al. Transforming gene from human stomach cancers and a noncancerous portion of stomach mucosa. Proc Natl Acad Sci U S A 1986;83:3997–4001.
16. Matsumoto S, Takahashi K, Iwakawa R, et al. Frequent EGFR mutations in brain metastases of lung adenocarcinoma. Int J Cancer 2006;119:1491–4.
17. Hamada K, Kohno T, Takahashi M, et al. Two regions of homozygous deletion clusters at chromosome band 9p21 in human lung cancer. Genes Chromosomes Cancer 2000;27:308–18.
18. Riely GJ, Politi KA, Miller VA, Pao W. Update on epidermal growth factor receptor mutations in non-small cell lung cancer. Clin Cancer Res 2006;12:7232–41.
19. Sakamoto H, Shimizu J, Horio Y, et al. Disproportionate representation of KRAS gene mutation in atypical adenomatous hyperplasia, but even distribution of EGFR gene mutation from preinvasive to invasive adenocarcinomas. J Pathol 2007;212:287–94.
20. Travis WD, Brambilla E, Muller-Hermelink HK, Harris CC, editors. Pathology and genetics: tumours of the lung, pleura, thymus and heart. Lyon: IARC Press; 2004. p. 73–5.
21. Aoyagi Y, Yokose T, Minami Y, et al. Accumulation of losses of heterozygosity and multistep carcinogenesis in pulmonary adenocarcinoma. Cancer Res 2001;61:7950–4.
22. Haneda H, Sasaki H, Shimizu S, et al. Epidermal growth factor receptor gene mutation defines distinct subsets among small adenocarcinomas of the lung. Lung Cancer 2006;52:47–52.

Jpn J Clin Oncol 2008;38(10)715–718
doi:10.1093/jjco/hyn095

Clinical Trial Note

A Multicenter Phase I Trial of Interferon-β and Temozolomide Combination Therapy for High-grade Gliomas (INTEGRA Study)

Toshihiko Wakabayashi[1], Takamasa Kayama[2], Ryo Nishikawa[3], Hiroshi Takahashi[4], Toshiki Yoshimine[5], Nobuo Hashimoto[6], Tomokazu Aoki[7], Kaoru Kurisu[8], Atsushi Natsume[1], Masatoshi Ogura[1] and Jun Yoshida[1]

[1]Department of Neurosurgery, Nagoya University School of Medicine, Nagoya, [2]Department of Neurosurgery, Yamagata University School of Medicine, Yamagata, [3]Department of Neurosurgery, Saitama Medical University, Saitama, [4]Department of Neurosurgery, Nippon Medical School, Tokyo, [5]Department of Neurosurgery, Osaka University School of Medicine, Osaka, [6]Department of Neurosurgery, Kyoto University School of Medicine, Kyoto, [7]Department of Neurosurgery, Kitano Hospital, Osaka and [8]Department of Neurosurgery, Hiroshima University School of Medicine, Hiroshima, Japan

Received June 24, 2008; accepted August 14, 2008

A multicenter phase I clinical trial, namely, Integrated Japanese Multicenter Clinical Trial: A Phase I Study of Interferon-β and Temozolomide for Glioma in Combination with Radiotherapy (INTEGRA Study), is being conducted for patients with high-grade glioma in order to evaluate the safety, feasibility and preliminary clinical effectiveness of the combination of interferon-β and temozolomide. The primary endpoint is incidence of adverse events. The secondary endpoints are progression-free survival time and overall survival time. In addition, objective tumor response will be evaluated in a subpopulation of patients with the measurable disease. The reduction rate of tumor will be calculated according to Response Evaluation Criteria In Solid Tumors for measurable tumors as determined by magnetic resonance imaging. Subsequently, the overall response will be evaluated based on the results of measurable and non-measurable tumors. Ten newly diagnosed and 10 recurrent patients will be enrolled in this study.

Key words: chemo-phase I-II-III – clinical trials – CNS

INTRODUCTION

Gliomas account for ~40% of all brain tumors and are thus the most common primary tumors of the central nervous system. Primary brain tumors are classified according to their cell type and histological grade into categories defined by the World Health Organization (WHO) (1). High-grade (WHO grades III and IV) gliomas, which include anaplastic astrocytoma (AA), anaplastic oligodendroglioma (AO), anaplastic oligoastrocytoma (AOA) and glioblastoma multiforme (GBM), are often resistant to treatment; GBM, the most common glioma in adults, kills patients within a median time span of a year after diagnosis despite treatment with aggressive surgical resection, nitrosourea-based chemotherapy and radiotherapy (2–4). A number of studies by large cooperative groups have shown the benefits of radiation therapy in doses up to 60 Gy after surgery for improving overall survival and time to progression (5). In Japan, nitrosourea agents such as 1-(4-amino-2-methyl-5-pyridiminyl)methyl-3-(2-chloroethyl)-3-nitrosourea and methyl-6-[3-(2-chloroethyl)-3-nitrosoureido]-6-deoxy-alpha-D-glucopyranoside have been used to treat malignant gliomas for a long time; however, this treatment offered few clinical benefits. Temozolomide (TMZ), an oral alkylating agent, has been demonstrated to possess antitumor activity against malignant gliomas, with minimal additional toxicity; furthermore, in a previous study of concomitant radiation therapy and chemotherapy with TMZ followed by adjuvant TMZ, survival duration substantially improved (6). In 2006, TMZ

For reprints and all correspondence: Toshihiko Wakabayashi, Department of Neurosurgery, Nagoya University School of Medicine, Nagoya, Japan.
E-mail: wakabat@med.nagoya-u.ac.jp

was certified as the treatment agent for malignant gliomas by the National Ministry of Health and Welfare of Japan, and a combination of radiotherapy and chemotherapy with TMZ is now used as the first-line therapy. However, its clinical outcomes depend on the *O*-(6)-methylguanine-DNA methyltransferase (MGMT) status, and MGMT modification is one of the key factors to obtain greater clinical benefits in the future.

Interferon-β (IFN-β) exhibits pleiotropic biological effects and has been widely used either alone or in combination with other antitumor agents in the treatment of malignant gliomas and melanomas (7). In the treatment of malignant gliomas, IFN-β can act as a drug sensitizer, enhancing toxicity against various neoplasms when administered in combination with nitrosourea. IFN-β and nitrosourea combination therapy has been particularly used for the treatment of gliomas in Japan (8). Previously, we demonstrated that IFN-β markedly enhanced chemosensitivity to TMZ in an *in vitro* study of human glioma cells (9); this finding suggested that one of the major mechanisms by which IFN-β enhances chemosensitivity is the downregulation of MGMT transcription via *p53* induction. This effect was also observed in an experimental animal model (10). These two studies suggested that chemotherapy with IFN-β and TMZ plus radiation might further improve the clinical outcome in malignant gliomas when compared with TMZ plus radiation therapy. Here, in order to evaluate the safety, feasibility and preliminary clinical effectiveness of the combination of IFN-β and TMZ, we are conducting a clinical study, namely, Integrated Japanese Multicenter Clinical Trial: A Phase I Study of Interferon-β and Temozolomide for Glioma in Combination with Radiotherapy (INTEGRA study). This study involves eight medical institutions, covering the entire regional population of Japan.

PROTOCOL DIGEST OF THE STUDY

Purpose

The main aim of this study is to evaluate the safety, feasibility and preliminary clinical effectiveness of IFN-β and TMZ for the treatment of malignant gliomas.

Study Setting and Protocol Review

This is a multicenter clinical trial involving eight neurosurgical institutions: Yamagata, Saitama Medical, Nippon Medical, Nagoya, Osaka, Kyoto, and Hiroshima Universities and Kitano Hospital. The protocol has been reviewed and approved by institutional review boards of each of these institutions.

Registration and Monitoring

Participating investigators are instructed to send an eligibility criteria report to the Data Center at Nagoya University, which is a third party different from the study director. Ten newly diagnosed and 10 recurrent patients are registered for a period of 6 months from December 2007. Data, including those of magnetic resonance imaging (MRI), blood tests, and pathology, will be collected at the data center. The quality of data will be checked and verified at the data center. If required, the data center would provide feedback to the institutions. The data center will send high-quality data to the study director. Committees of safety and efficacy (Dr Kazuo Tabuchi, Koyanagi Memorial Hospital, Saga), radiotherapy (Dr Shinji Naganawa, Department of Radiology, Nagoya University School of Medicine), pathological review (Dr Youichi Nagasato, Department of Pathology, Gunma University School of Medicine) and statistics (Dr Kunihiko Hayashi, Gunma University School of Health Science) will send their reports to the head office.

Endpoints

The primary endpoint is incidence of adverse events. The secondary endpoints are progression-free survival time and overall survival time. In addition, objective tumor response will be evaluated in a subpopulation of patients with measurable disease. The reduction rate of tumor will be calculated according to Response Evaluation Criteria In Solid Tumors for measurable tumors as determined by MRI. Non-measurable tumors are classified into four grades: complete remission, partial response, progression and not evaluable. Subsequently, the overall response will be evaluated based on the results of measurable and non-measurable tumors.

Eligibility Criteria

The eligibility criteria are as follows:

(i) Histologically confirmed diagnosis of newly diagnosed or recurrent high-grade glioma (AA, AO, AOA or GBM). More than 50% volume of tumor is located in the supratentorial region.
(ii) No tumor recognized in the optic nerve, olfactory nerve and pituitary gland on pretreatment MRI.
(iii) No dissemination detected by MRI. Age between 18 and 75 years at the time of registration.
(iv) Performance status is 0–2, 3 only due to neurological deficits.
(v) Sufficient organ function before chemotherapy according to the following laboratory data: WBC $\geq$ 3000/mm^3 or neutrophils $\geq$1500/mm^3, platelets $\geq$100 000/mm^3, hemoglobin $\geq$8.0 g/dl, bilirubin $\leq$1.5 mg/dl, serum glutamic oxaloacetic transaminase $\leq$ 100 IU, serum glutamic pyruvic transaminase $\leq$ 100 IU, creatinine $\leq$1.5 mg/dl, creatinine clearance $\geq$50 ml/min and electrocardiogram showing no serious arrhythmia and no serious ischemic heart disease.
(vi) No prior chemoradiotherapy for newly diagnosed patients.

(vii) The interval from the end of prior anti-tumor therapy (e.g. chemotherapy, radiotherapy, immunotherapy) must be at least 4 weeks for recurrent patients, regardless of the regimen.
(viii) Written informed consent.

Exclusion Criteria

The exclusion criteria are as follows:

(i) synchronous double cancer or metachronous double cancer in last 5 years; carcinoma *in situ* accepted;
(ii) meningitis or pneumonia;
(iii) pregnant, possibly pregnant, or nursing women;
(iv) mental disorder;
(v) uncontrolled diabetes mellitus (DM) or under treatment with insulin for DM;
(vi) myocardial infarction in last 3 months;
(vii) history of pulmonary fibrosis or interstitial pneumonia.

Treatment Methods

For newly diagnosed patients:

Radiotherapy 60 Gy/30 fr, 2 Gy ×5 days/week;
IFN-β 3 MIU/body, administered intravenously on alternate days during radiotherapy;
TMZ 75 mg/(m^2 day), daily from the first day to the last day of radiotherapy.

After completing this induction period, all patients will have 4 weeks of washout period, and they will be then shifted to adjuvant period.

IFN-β 3 MIU/body, administered on the first day morning every 4 weeks;
TMZ 150 mg/(m^2 day) (days 1–5: first cycle);
200 mg/(m^2 day) (days 1–5: second to sixth cycle).

In the absence of hematologic toxicity, the dose is increased to 200 mg/(m^2 day), beginning with the second cycle to the sixth cycle.

This cycle is repeated six times every 28 days in the absence of tumor progression, serious adverse events such as grade 4 hematological toxicity, refusal of therapy and deviation from the protocol.

For recurrent patients:

IFN-β 3 MIU/body, administered the first day morning every 4 weeks (day 1);
TMZ 150 mg/(m^2 day) (days 1–5: first cycle);
200 mg/(m^2 day) (days 1–5: second to sixth cycle).

In the absence of hematologic toxicity, the dose is increased to 200 mg/(m^2 day), beginning with the second cycle to the sixth cycle.

This cycle is repeated six times every 28 days.

This regimen has been considered to be the most promising based on previous clinical studies (8,11–14). Thus, dose-limiting toxicity was not evaluated in this study.

Follow-up and Statistical Methods

Disease progression and occurrence of new disease will be examined by MRI performed at baseline and at least after every 4–5 weeks during treatment. Blood tests and symptom checks will be carried out before treatment and at least after every 2 weeks during treatment. Follow-up will continue for 3 months from the end of treatment. In cases wherein therapy is discontinued due to toxicity, clinicians would follow-up patients until they recover from toxicity. In addition, overall survival, progression-free survival and treatment success curves are constructed as time-to-event plots by the Kaplan–Meier method.

Acknowledgement

We would like to thank Dr Junichi Sakamoto for his helpful comments and suggestions.

Funding

This work was supported in part by Japan Brain Foundation.

Conflict of interest statement

None declared.

References

1. Louis DN, Ohgaki H, Wiestler OD, Cavenee WK, Burger PC, Jouvet A, et al. The 2007 WHO classification of tumours of the central nervous system. *Acta Neuropathol* 2007;114:97–109.
2. Nagane M, Levitzki A, Gazit A, Cavenee WK, Huang HJ. Drug resistance of human glioblastoma cells conferred by a tumor-specific mutant epidermal growth factor receptor through modulation of Bcl-XL and caspase-3-like proteases. *Proc Nat Acad Sci USA* 1998;95:5724–9.
3. Ohgaki H, Dessen P, Jourde B, Horstmann S, Nishikawa T, Di Patre PL, et al. Genetic pathways to glioblastoma: a population-based study. *Cancer Res* 2004;64:6892–9.
4. Ohgaki H, Kleihues P. Population-based studies on incidence, survival rates, and genetic alterations in astrocytic and oligodendroglial gliomas. *J Neuropathol Exp Neurol* 2005;64:479–89.
5. Walker MD, Green SB, Byar DP, Alexander E Jr, Batzdorf U, Brooks WH, et al. Randomized comparisons of radiotherapy and nitrosoureas for the treatment of malignant glioma after surgery. *N Engl J Med* 1980;303:1323–9.
6. Stupp R, Mason WP, van den Bent MJ, Weller M, Fisher B, Taphoorn MJ, et al. Radiotherapy plus concomitant and adjuvant temozolomide for glioblastoma. *N Engl J Med* 2005;352:987–96.
7. Chawla-Sarkar M, Lindner DJ, Liu YF, Williams BR, Sen GC, Silverman RH, et al. Apoptosis and interferons: role of interferon-stimulated genes as mediators of apoptosis. *Apoptosis* 2003;8:237–49.
8. Wakabayashi T, Hatano N, Kajita Y, Yoshida T, Mizuno M, Taniguchi K, et al. Initial and maintenance combination treatment with interferon-beta, MCNU (Ranimustine), and radiotherapy for patients with previously untreated malignant glioma. *J Neurooncol* 2000;49:57–62.

9. Natsume A, Ishii D, Wakabayashi T, Tsuno T, Hatano H, Mizuno M, et al. IFN-beta down-regulates the expression of DNA repair gene MGMT and sensitizes resistant glioma cells to temozolomide. *Cancer Res* 2005;65:7573–9.
10. Natsume A, Wakabayashi T, Ishii D, Maruta H, Fujii M, Shimato S, et al. A combination of IFN-beta and temozolomide in human glioma xenograft models: implication of p53-mediated MGMT downregulation. *Cancer Chemother Pharmacol* 2007.
11. Aoki T, Takahashi JA, Ueba T, Oya N, Hiraoka M, Matsui K, et al. Phase II study of nimustine, carboplatin, vincristine, and interferon-beta with radiotherapy for glioblastoma multiforme: experience of the Kyoto Neuro-Oncology Group. *J Neurosurg* 2006;105:385–91.
12. Hatano N, Wakabayashi T, Kajita Y, Mizuno M, Ohno T, Nakayashiki N, et al. Efficacy of post operative adjuvant therapy with human interferon beta, MCNU and radiation (IMR) for malignant glioma: comparison among three protocols. *Acta Neurochir* 2000;142:633–8; discussion 9.
13. Watanabe T, Katayama Y, Yoshino A, Fukaya C, Yamamoto T. Human interferon beta, nimustine hydrochloride, and radiation therapy in the treatment of newly diagnosed malignant astrocytomas. *J Neurooncol* 2005;72:57–62.
14. Yoshida J, Kajita Y, Wakabayashi T, Sugita K. Long-term follow-up results of 175 patients with malignant glioma: importance of radical tumour resection and postoperative adjuvant therapy with interferon, ACNU and radiation. *Acta Neurochir* 1994;127:55–9.

J Neurosurg 109:867–873, 2008

Convection-enhanced delivery of polyethylene glycol–coated liposomal doxorubicin: characterization and efficacy in rat intracranial glioma models

Laboratory investigation

Toshio Kikuchi, M.D.,[1] Ryuta Saito, M.D., Ph.D.,[1] Shin-ichirou Sugiyama, M.D.,[1] Yoji Yamashita, M.D., Ph.D.,[1] Toshihiro Kumabe, M.D., Ph.D.,[1] Michal Krauze, M.D.,[2] Krystof Bankiewicz, M.D., Ph.D.,[2] and Teiji Tominaga, M.D., Ph.D.[1]

[1]*Department of Neurosurgery, Tohoku University Graduate School of Medicine, Sendai, Miyagi, Japan; and* [2]*Department of Surgical Neurology, University of California, San Francisco, California*

Object. The characteristics of polyethylene glycol–coated liposomal doxorubicin (PLD), the only liposomal drug now clinically available for intravenous injection, were investigated after convection-enhanced delivery (CED) into the rat brain parenchyma.

Methods. The distribution, tissue retention, and toxicity profile were evaluated after CED into the rat brain parenchyma. The antitumor efficacy was also determined in rodent intracranial U-251MG and U-87MG glioma models.

Results. Convection-enhanced delivery of PLD achieved wider distributions and delayed onset of toxicity in the brain parenchyma compared with CED of free doxorubicin infusion. Fluorescence generated from doxorubicin infused as PLD was detected until at least 30 days after infusion. Local toxicity was not observed when a 10% dilution of the commercially available PLD solution was used (0.2 mg/ml doxorubicin), but was significant at higher concentrations. Results after 10% PLD was delivered locally with CED demonstrated significant survival prolongation in both intracranial U-251MG and U-87MG xenograft models.

Conclusions. Convection-enhanced delivery of PLD achieved extensive tissue distribution and sustained drug release. Convection-enhanced delivery of PLD is a promising chemotherapy for the treatment of malignant gliomas. *(DOI: 10.3171/JNS/2008/109/11/0867)*

Key Words • **chemotherapy** • **convection-enhanced delivery** • **glioma** • **liposomal doxorubicin** • **rat**

Chemotherapy for malignant gliomas remains a challenging field for researchers because of the chemoresistance often observed in these lesions.[4] Poor drug delivery is one explanation, caused by the hindrance of the blood–brain and blood–tumor barriers to the entry of chemotherapeutic agents administered systemically. Consequently, even in optimal situations, only a small fraction of the administered drug actually reaches the tumor cells. Local drug delivery is therefore a promising strategy for overcoming the chemoresistance of malignant glioma, as local administration results in 100% dose delivery to the target site. For example, Gliadel wafers (poly [carboxyphenoxy-propane/sebacic acid] anhydride wafers) are designed to release their 3.85% carmustine (1,3-bis-chlorethyl-1-nitrosourea) content slowly over a 2–3-week period after implantation on the surface of the tumor resection cavity. Authors of recent studies have demonstrated life-prolonging efficacy of Gliadel wafers against recurrent and primary malignant gliomas.[2,17] However, the major disadvantage to this method is the drug's limited distribution, as high-dose delivery occurs only within mm of the implant.[3] Therefore, a drug delivery method that achieves extensive distribution of the therapeutic agent together with slow-release capability may further improve the therapeutic efficacy.[12,13]

Convection-enhanced delivery is a relatively new drug delivery method that might overcome the problems of local drug delivery. This technique uses a pressure gradient established at the tip of an infusion catheter to create the bulk flow that pushes the drug through the interstitial space.[1]

Abbreviations used in this paper: CED = convection-enhanced delivery; PBS = phosphate-buffered saline; PLD = polyethylene glycol–coated liposomal doxorubicin.

We previously reported the efficacy of PLD delivered via CED in the rodent intracranial U-251MG glioma xenograft model.[18] Polyethylene glycol–coated liposomal doxorubicin is a liposomal drug approved for systemic intravenous delivery against breast cancer, ovarian cancer, and others.[8,10] Convection-enhanced delivery of PLD has been shown to be more effective than systemic delivery of the maximum tolerable dose, and CED of free doxorubicin.[18]

In the present study, we investigated the distribution, sustained release, and toxicity of PLD after CED in the normal rat brain parenchyma. Antitumor efficacy was also evaluated in the well-established rodent intracranial U-251MG and U-87MG xenograft models.[9]

Methods

Free Doxorubicin and PLD

Stock solutions of free doxorubicin (Sigma) were prepared by diluting the doxorubicin in dimethyl sulfoxide to a concentration of 50 mg/ml. The infusion solutions of free doxorubicin were made by diluting the stock solution with PBS. The infusion solution containing 4% dimethyl sulfoxide had no toxicity when 20 μl was infused by CED (data not shown). Polyethylene glycol–coated liposomal doxorubicin (Doxil [doxorubicin hydrochloride liposome], ALZA Corporation) was obtained commercially via iRxMedicine, Oz International Inc. The commercial PLD solutions contained 2 mg/ml of doxorubicin. The infusion solution was made by diluting the stock solution with PBS.

Tumor Cell Lines

The established human glioblastoma multiforme cell line, U-251MG, was obtained from the Brain Tumor Research Center Tissue Bank at the University of California, San Francisco. The U-87MG human glioblastoma cell line was purchased from the American Type Culture Collection. Cells were maintained as monolayers in a complete medium consisting of Eagle minimum essential medium supplemented with 10% fetal bovine serum and nonessential amino acids. Cells were cultured in an incubator at 37°C in a humidified atmosphere composed of 95% air and 5% carbon dioxide.

Experimental Animals

Seven-week-old male Fischer 344 rats were purchased from Japan SLC, Inc. Seven-week-old male Fischer 344/NJcl-rnu/rnu (nude) rats were purchased from CLEA Japan, Inc. Male Sprague–Dawley rats weighing ~ 250 g were obtained from Charles River Laboratories. Congenitally athymic, male nude rats (rnu/rnu, homozygous) weighing ~ 150–200 g were purchased from the National Cancer Institute. Protocols used in the animal studies were approved either by the Institute for Animal Experimentation, Tohoku University Graduate School of Medicine, or by the Institutional Animal Care and Use Committee, University of California, San Francisco.

Intracranial Tumor Model

Cells were harvested by trypsinization, washed once with complete medium, and suspended in Ca^{++}- and Mg^{++}-free PBS for implantation. A cell suspension containing 50×10^4 cells/10 μl in PBS was prepared for implantation. Fischer 344/NJcl-rnu/rnu (nude) rats were used for the U-87MG xenograft model, and nude rats (rnu/rnu, homozygous) were used for the U-251MG xenograft model. Under deep halothane anesthesia, the rats were placed in small-animal stereotactic frames (Narishige Co.). A sagittal incision was made through the skin to expose the cranium, and a bur hole was made with a small drill in the skull 0.5-mm anterior and 3-mm lateral to the bregma. At a depth of 4.5 mm from the brain surface, 5 μl of the cell suspension was injected. After 2 minutes, another 5 μl was injected at a depth of 4 mm and after another 2 minutes, the implantation needle was removed and the wound sutured.

Convection-Enhanced Delivery

The infusion was performed using the CED method as described previously.[11] A reflux-free infusion cannula consisting of a fine silica tube and a 27-gauge metal needle[6] was connected to the syringe placed on a microinfusion pump (BeeHive, Bioanalytical System) to control the infusion rate. The infusion proceeded at 0.2 μl/minute for 15 minutes, 0.5 μl/minute for 10 minutes, and 0.8 μl/minute for 15 minutes, for a total infusion 20 μl in 40 minutes. The therapeutic agent was infused locally at a 4.0-mm depth using the same stereotactic coordinates at 7 days after tumor implantation.

Detection of Doxorubicin

The drug distribution after CED was analyzed in 3 Fischer 344 rats that received 20 μl of 10% PLD (0.2 mg/ml doxorubicin) into the striatum. The rats were killed immediately after CED, and their brains harvested and frozen in dry ice–cooled isopentane. The fresh frozen brains were cut into 25-μm-thick coronal sections on a cryostat, and the sections were placed on microscope slides. Fluorescence generated from the doxorubicin with ultraviolet illumination was visualized under a fluorescent microscope and captured by a charge-coupled device camera (DFC350 FX, Leica Microsystems). To compare tissue distributions and toxicity onset after CED and PLD or free doxorubicin, 6 Sprague–Dawley rats received 100% PLD (2.0 mg/ml doxorubicin) in the right hemisphere and 2.0 mg/ml free doxorubicin in the left hemisphere. Three of these rats were killed 1 hour after infusion, and the other 3 were killed 5 days after infusion. The fresh frozen brains were observed under fluorescence and light microscopy.

Tissue Retention and Toxicity After CED

The clearance of PLD in rat brains was investigated in 8 normal Fischer 344 rats that received 20 μl of 10% PLD (0.2 mg/ml doxorubicin). Two rats were killed at 7, 14, 30, and 60 days after infusion, and their brains were processed for histological detection of fluorescence. The brain section with the highest fluorescence intensity was photographed with a charge-coupled device camera. The toxicity on normal brain parenchyma of the PLD delivered locally via CED was evaluated in 12 Fischer 344

rats divided into 4 groups according to type of 20-μl infusion: the sham surgery group received PBS, and the other 3 groups received 10% PLD (0.2 mg/ml doxorubicin), 20% PLD (0.4 mg/ml doxorubicin in concentration), or 100% PLD (2.0 mg/ml doxorubicin). Body weight was measured before CED and then weekly thereafter. Sixty-three days after CED, the rats were killed, perfused with 10% formalin, and the brains processed for histological examination with H & E staining.

Survival Study

Seven days after implantation, 12 rats with U-251MG tumor cells and 14 with U-87MG tumor cells were randomly divided into 2 groups: a sham surgery group that underwent CED of PBS (6 rats with U-251MG and 7 with U-87MG cells), and a group that underwent CED of 10% PLD (0.2 mg/ml doxorubicin; 6 rats with U-251MG and 7 with U-87MG cells). All rats were carefully observed for general health and survival.

Statistical Analysis

Animal survival was plotted using the Kaplan–Meier method. Differences in survival were determined using the log-rank test and probability values < 0.05 were considered statistically significant. Commercially available software (StatMate software, ATMS Co., Ltd.) was used for statistical analysis.

Results

Distribution of PLD in Brain Parenchyma

Effective distribution of PLD was confirmed in the rodent brain. Representative serial sections obtained at 1-mm intervals are shown in Fig. 1. Fluorescence generated from doxorubicin by ultraviolet illumination demonstrated extensive distribution of PLD after CED. Similar distributions were found in all 3 rats tested.

Tissue Distribution and Onset of Toxicity of PLD and Free Doxorubicin After CED

At 1 hour after infusion, slight damage to the brain at the site of the infusion was observed only in the left hemisphere that had received free doxorubicin. Distributions of PLD were much larger than those of free doxorubicin (Fig. 2A). Five days after infusion, severe local toxicity was found in the left hemisphere that had received free doxorubicin, whereas only slight tissue changes were found in right hemisphere that received PLD. Diffuse fluorescence from doxorubicin was found in the normal brain tissue surrounding the necrotic cavity of the hemisphere that had received free doxorubicin, probably causing more severe side effects. In contrast, in the hemisphere that received PLD the fluorescence remained mostly at the same site as observed within 1 hour of the infusion (Fig. 2B).

Tissue Retention of PLD After CED

Based on the late onset of toxicity found in the hemisphere that received PLD, we evaluated the duration of tissue retention of PLD using a 10% dilution of the stock solution (0.2 mg/ml doxorubicin). Fluorescence generated from doxorubicin by ultraviolet illumination was detected in rodent brains at 7, 14, 30, and 60 days after CED (Fig. 3). The signal intensity remained high until 14 days after CED, but then gradually decreased. Only faint fluorescence was detectable in the brain parenchyma by 60 days after infusion.

Toxicity of PLD in Normal Rodent Brain

Because the fluorescence generated from doxorubicin had diminished by 60 days after infusion, toxicity analysis was continued until 63 days after infusion. All rats that had received PLD in any concentration by CED gained body weight steadily at the same rate as the control rats until 63 days postinfusion (Fig. 4A). Daily observations also revealed no clinical deficits in all rats during the 63-day observation period. All rats were killed at 63 days after infusion of PLD, and their brains were processed (Fig. 4B). Histological examination revealed brain tissue damage in rat brains that received 0.4 mg/ml doxorubicin as PLD (20% dilution) or above. The 3 rats that received 0.2 mg/ml doxorubicin as PLD survived without clinical symptoms until 63 days after infusion, and brain tissue damage was almost negligible.

Antitumor Efficacy of PLD Infused by CED

Because 10% PLD was the maximum dose that did

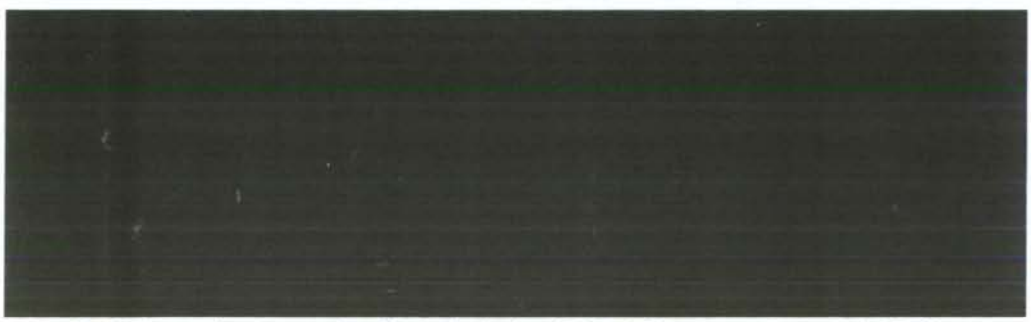

FIG. 1. Tissue sections demonstrating effective distribution of PLD by CED in the normal rodent brain. The 25-μm thick sections obtained at 1-mm intervals were examined with a fluorescence microscope to detect the signals generated from doxorubicin with ultraviolet illumination. Original magnification × 12.5.

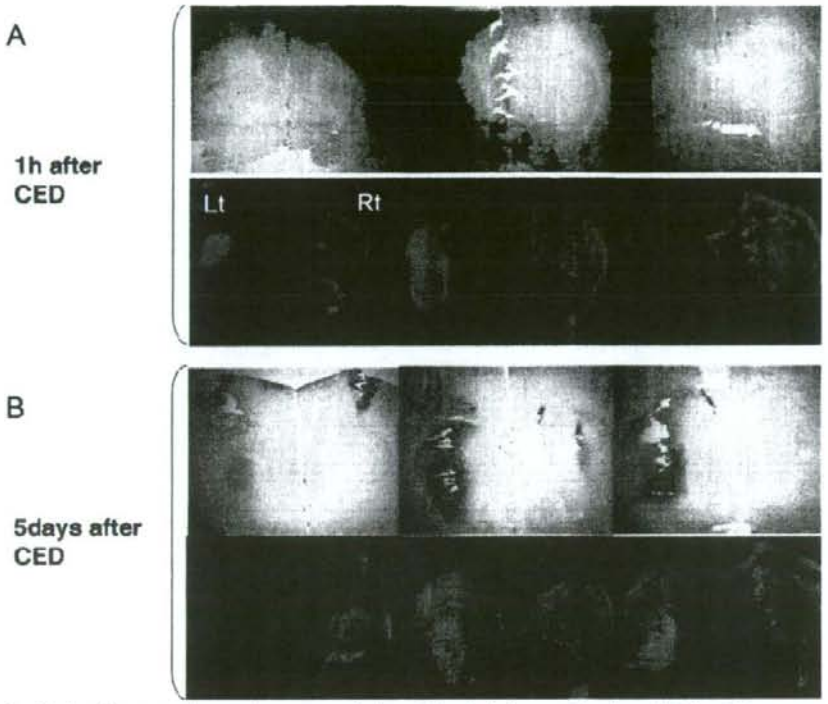

FIG. 2. Light microscopy images (*upper rows* in A and B; original magnification × 12.5) and fluorescence microscopy images detecting fluorescence generated from doxorubicin with ultraviolet illumination (*lower rows* in A and B). Images show tissue distribution of PLD *(right hemisphere)* or free doxorubicin *(left hemisphere)* after CED in 6 rats. Three rats were killed 1 hour after infusion (A) and 3 others were killed 5 days after infusion (B). Three sequential 25-μm sections at 1-mm intervals from a representative rat at each time point are shown.

not cause damage to normal brain tissue, this concentration was used in the survival study (Fig. 5).

Among the rats in the U-251MG xenograft model, those in the sham surgery group that received CED of PBS were all killed 41–45 days after tumor cell implantation because of neurological symptoms indicative of tumor progression. Five of 6 rats that received 0.2 mg/ml doxorubicin as PLD by CED had to be killed 55–67 days after tumor implantation, and 1 rat lived until the end of this study. Formation of large tumors was verified in all rats killed in these groups. The survival of rats that received 0.2 mg/ml doxorubicin as PLD was significantly longer than in rats that underwent mock surgery ($p = 0.0006$, log-rank test).

The U-87MG rats in the mock surgery group were all killed 15 to 16 days after tumor cell implantation because of neurological symptoms indicative of tumor progression. All rats that received 0.2 mg/ml doxorubicin as PLD by CED had to be killed 14–19 days after tumor implantation. Formation of large tumors was verified in all rats killed in these groups. The survival of rats that received 0.2 mg/ml doxorubicin as PLD was significantly

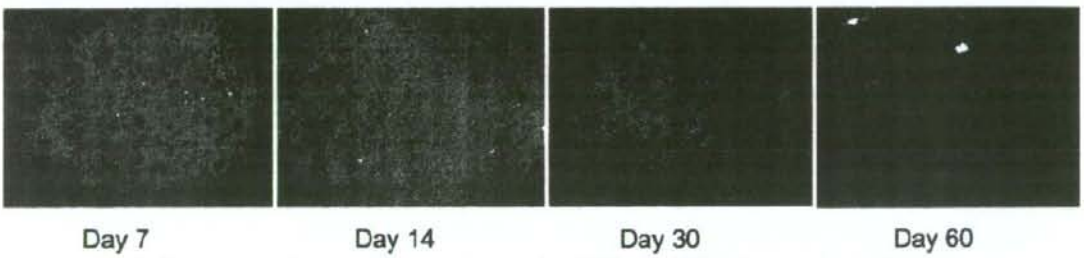

FIG. 3. Fluorescence microscopy demonstrating retention of PLD after CED in the normal rodent brain. Fluorescence was strongly observed for 14 days after infusion but then diminished. Sixty days after infusion, the fluorescence had almost faded away and was hardly detectable. Original magnification × 50.

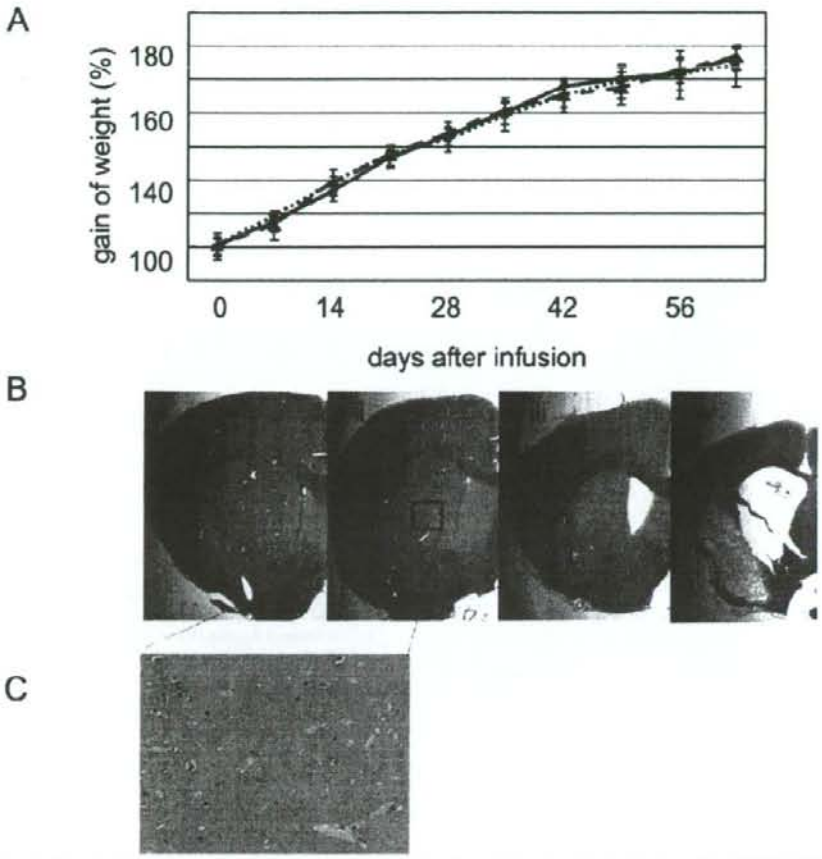

FIG. 4. A: Graph demonstrating weight gain observed during the study period in rats that received PBS *(solid line)*, 10% PLD *(dotted line)*, and 100% PLD *(dashed line)*. The 20% PLD group is not shown. All rats gained weight at the same rate. B: Photomicrographs obtained 63 days after infusion revealing local tissue damage and atrophy of the infused hemisphere in all groups (i, control; ii, 10% PLD; iii, 20% PLD; and iv, 100% PLD). C: Higher magnification photomicrograph of *boxed area*. Original magnification × 12.5 (B) and × 100 (C).

longer than in the mock surgery group ($p = 0.016$, log-rank test).

Discussion

Polyethylene glycol–coated liposomal doxorubicin is formulated with surface-bound polyethylene glycol to protect the liposomes from detection by the monocytes and macrophages in the liver and spleen after systemic delivery. The pharmacokinetics of PLD compared with those of free doxorubicin involve a prolonged circulation time, increased accumulation in the tumor, sustained drug release, and reduced systemic side effects. Intravenous administration of PLD resulted in enhanced drug exposure and improved therapeutic efficacy in a rodent brain glioma model.[15] Intravenous injection of PLD is safe and moderately effective in patients with recurrent high-grade gliomas.[5] Local intratumoral administration of free doxorubicin appeared to be safe and effective in 10 patients suffering high-grade gliomas.[16] Considering these previous data, local administration of PLD may have therapeutic advantages compared with free drug administration.

Convection-enhanced delivery can achieve extensive distribution of the locally applied agents, and CED of liposomal agents with slow-release capability may achieve ideal drug delivery for malignant gliomas. Liposomes were extensively distributed after CED into the brain parenchyma in the present (Fig. 1) and in previous studies.[7,11] The distribution of PLD was more extensive than that of free doxorubicin (Fig. 2). This finding is consistent with our previous observation that free doxorubicin is immediately absorbed in the nuclei, whereas PLD diffuses through the intercellular space, resulting in wider distribution.[14] Free-drug infusion by CED into the striatum damaged the brain more rapidly than PLD infused by CED. A large area of tissue necrosis was observed at

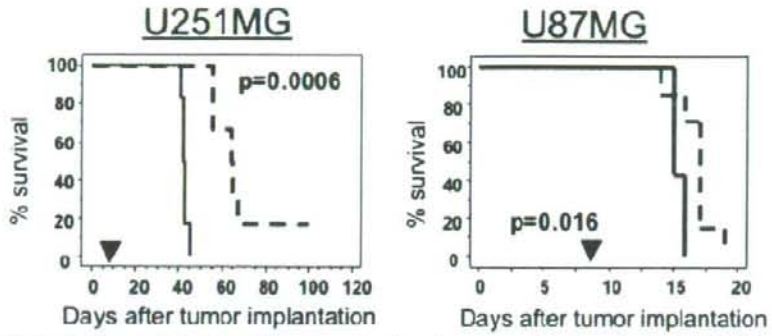

FIG. 5. Kaplan–Meier survival plots of 12 nude rats (rnu/rnu, homozygous) implanted with U-251MG tumor cells and 14 Fischer 344/NJcl-rnu/rnu (nude) rats implanted with U-87MG tumor cells and divided into 2 groups: a sham surgery group (*solid lines*), and a group that received CED of PLD (0.2 mg/ml doxorubicin; *dotted lines*). Seven days after tumor cell implantation, CED of 20-μl PBS or drug infusion was performed. Rats were killed after developing neurological symptoms indicative of tumor progression. The survival of the rats that received 0.2 mg/ml doxorubicin as PLD was significantly longer than those that received mock surgery ($p = 0.0006$ in U-251MG model, $p = 0.016$ in U-87MG model; log-rank test).

the initial distribution area in the brain tissue exposed to free doxorubicin, whereas only slight tissue damage was observed adjacent to the needle tract in the brain tissue exposed to PLD (Fig. 2). Sixty-three days after infusion, however, the 100% PLD infusion (2 mg/ml doxorubicin) had damaged the tissue throughout the hemisphere (Fig. 4), indicating the slow release capacity of liposomes. Fluorescence generated from doxorubicin could be detected at least 30 days after infusion (Fig. 3). These findings indicate that PLD achieved wide distribution and sustained release of doxorubicin in the brain parenchyma.

In the survival studies 10% PLD was used, containing 0.2 mg/ml doxorubicin, which was defined as the safe dose for local administration. Significant prolongation of survival was observed in the intracranial U-251MG xenograft model.[18] Similar but less significant survival prolongation was observed in the intracranial U-87MG xenograft model. This difference may depend on the cellular sensitivity to doxorubicin, or on the life spans of the rats in these models. The life expectancy in the U-251MG xenograft model rats was 42.7 ± 1.4 days, whereas that in the U-87MG model rats was 15.4 ± 0.5 days. Therefore, the life span of the U-87MG rats might not allow testing of the efficacy of the proposed treatment. Humans with gliomas have a much longer life expectancy, so this treatment strategy may achieve better efficacy.

Conclusions

Convection-enhanced delivery of PLD achieved wide distribution and slow release of the encapsulated doxorubicin in the brain parenchyma of the rat. Polyethylene glycol–coated liposomal doxorubicin administered at a dose safe to the normal brain tissue demonstrated significant survival prolongation effects in rodent intracranial glioma xenograft models. Convection-enhanced delivery of PLD is a promising treatment for malignant gliomas.

Disclaimer

The authors report no conflict of interest concerning the materials or methods used in this study or the findings specified in this paper.

References

1. Bobo RH, Laske DW, Akbasak A, Morrison PF, Dedrick RL, Oldfield EH: Convection-enhanced delivery of macromolecules in the brain. **Proc Natl Acad Sci U S A 91:**2076–2080, 1994
2. Brem H, Piantadosi S, Burger PC, Walker M, Selker R, Vick NA, et al: Placebo-controlled trial of safety and efficacy of intraoperative controlled delivery by biodegradable polymers of chemotherapy for recurrent gliomas. **Lancet 345:**1008–1012, 1995
3. Fleming AB, Saltzman WM: Pharmacokinetics of the carmustine implant. **Clin Pharmacokinet 41:**403–419, 2002
4. Groothuis DR: The blood-brain and blood-tumor barriers: a review of strategies for increasing drug delivery. **Neuro Oncol 2:**45–59, 2000
5. Hau P, Fabel K, Baumgart U, Rummele P, Grauer O, Bock A, et al: Pegylated liposomal doxorubicin-efficacy in patients with recurrent high-grade glioma. **Cancer 100:**1199–1207, 2004
6. Krauze MT, Saito R, Noble C, Tamas M, Bringas J, Park JW, et al: Reflux-free cannula for convection-enhanced high-speed delivery of therapeutic agents. **J Neurosurg 103:**923–929, 2005
7. Mamot C, Nguyen JB, Pourdehnad M, Hadaczek P, Saito R, Bringas JR, et al: Extensive distribution of liposomes in rodent brains and brain tumors following convection-enhanced delivery. **J Neurooncol 68:**1–9, 2004
8. O'Shaughnessy JA: Pegylated liposomal doxorubicin in the treatment of breast cancer. **Clin Breast Cancer 4:**318–328, 2003
9. Ozawa T, Wang J, Hu LJ, Bollen AW, Lamborn KR, Deen DF: Growth of human glioblastomas as xenografts in the brains of athymic rats. **In Vivo 16:**55–60, 2002
10. Perez-Lopez ME, Curiel T, Gomez JG, Jorge M: Role of pegylated liposomal doxorubicin (Caelyx) in the treatment of relapsing ovarian cancer. **Anticancer Drugs 18:**611–617, 2007
11. Saito R, Bringas JR, McKnight TR, Wendland MF, Mamot C, Drummond DC, et al: Distribution of liposomes into brain and rat brain tumor models by convection-enhanced delivery monitored with magnetic resonance imaging. **Cancer Res 64:**2572–2579, 2004

12. Saito R, Krauze MT, Bringas JR, Noble C, McKnight TR, Jackson P, et al: Gadolinium-loaded liposomes allow for real-time magnetic resonance imaging of convection-enhanced delivery in the primate brain. **Exp Neurol 196**:381–389, 2005
13. Saito R, Krauze MT, Noble CO, Drummond DC, Kirpotin DB, Berger MS, et al: Convection-enhanced delivery of Ls-TPT enables an effective, continuous, low-dose chemotherapy against malignant glioma xenograft model. **Neuro Oncol 8**: 205–214, 2006
14. Saito R, Krauze MT, Noble CO, Tamas M, Drummond DC, Kirpotin DB, et al: Tissue affinity of the infusate affects the distribution volume during convection-enhanced delivery into rodent brains: implications for local drug delivery. **J Neurosci Methods 154**:225–232, 2006
15. Siegal T, Horowitz A, Gabizon A: Doxorubicin encapsulated in sterically stabilized liposomes for the treatment of a brain tumor model: biodistribution and therapeutic efficacy. **J Neurosurg 83**:1029–1037, 1995
16. Voulgaris S, Partheni M, Karamouzis M, Dimopoulos P, Papadakis N, Kalofonos HP: Intratumoral doxorubicin in patients with malignant brain gliomas. **Am J Clin Oncol 25**: 60–64, 2002
17. Westphal M, Hilt DC, Bortey E, Delavault P, Olivares R, Warnke PC, et al: A phase 3 trial of local chemotherapy with biodegradable carmustine (BCNU) wafers (Gliadel wafers) in patients with primary malignant glioma. **Neuro Oncol 5**:79–88, 2003
18. Yamashita Y, Saito R, Krauze MT, Kawaguchi T, Noble CO, Drummond DC, et al: Convection-enhanced delivery of liposomal doxorubicin in intracranial brain tumor xenografts. **Targeted Oncol 1**:79–85, 2006

Manuscript submitted June 28, 2007.
Accepted November 30, 2007.

Address correspondence to: Ryuta Saito, M.D., Ph.D., Department of Neurosurgery, Tohoku University Graduate School of Medicine, 1-1 Seiryo-machi, Aoba-ku, Sendai 980-8574, Japan. email: ryuta@nsg.med.tohoku.ac.jp.

No Shinkei Geka, 36(11): 1005 - 1010, 2008

テクニカル・ノート ◆ Technical Note

パルスレーザージェットメス—神経膠腫手術への臨床応用*

中川 敦寛[1], 隈部 俊宏[1], 金森 政之[1], 斎藤 竜太[1], 平野 孝幸[1],
高山 和喜[2], 冨永 悌二[1]

Clinical Application of Pulsed Laser-induced Liquid Jet: Preliminary Report in Glioma Surgery

Atsuhiro NAKAGAWA[1], Toshihiro KUMABE[1], Masayuki KANAMORI[1], Ryuta SAITO[1], Takayuki HIRANO[1], Kazuyoshi TAKAYAMA[2], and Teiji TOMINAGA[1]

Key words:
glioma,
microsurgery,
minimally invasive neurosurgery,
water jet

Purpose: Both maximum resection of tumor and preservation of fine vessels are conflicting aims, but important factors to improve outcome in glioma surgery. Water jet dissection has been reported to dissect tissue while ensuring preservation of fine vessels. However, it was difficult to apply conventional water jet device in microsurgery due to the use of high pressure and continuous water a flow. To overcome these issues, we have developed pulsed holmium: yttrium-aluminum-garnet (YAG) laser-induced liquid jet (LILJ) for microsugical use and applied it in glioma surgery.

Methods: LILJ was generated by irradiating pulsed Ho: YAG laser (3 Hz, pulse laser energy 233-300 mJ/pulse) within a stainless tube (outer diameter (OD): 1.26 mm inner diameter (ID): 0.90 mm) filled with cold (4°C) lactated Ringer's solution. The laser beam was conducted through optical quartz fiber (core diameter: 400 μm). The jet generated was ejected from a stainless nozzle (OD: 1.06 mm, ID: 0.70 mm). To avoid splash and air bubbles within the surgical field, the nozzle was placed inside a stainless suction tube (OD: 3.06 mm, ID: 2.64 mm). LILJ was ejected randomly toward blood vessels and tissue simultaneously after removal of arachnoid membrane by microsurgical technique, and the quality of the dissection and the visual field were evaluated in 4 patients with supratentorial glioma.

Results: Restoration of small arteries (diameter: 100 to 200 microns) was accomplished. There was no significant occurrence of splash or air bubbles under the microscopic view.

Conclusion: Present results showed that the pulsed LILJ system may safely be used for microsurgical procedures, and may be useful for glioma resection where preservation of fine vessels is required.

(Received : December 17, 2007, Accepted : July 7, 2008)

No Shinkei Geka 36(11): 1005 - 1010, 2008

*(2007. 12. 17 受稿, 2008. 7. 7 受理)

1) 東北大学大学院医学系研究科神経外科学分野, Department of Neurosurgery, Tohoku University Graduate School of Medicine
2) 東北大学先進医工学連携機構ナノメディスン分野, Nanomedicine, Tohoku University Biomedical Engineering Organization
〔連絡先〕中川敦寛＝東北大学大学院医学系研究科神経外科学分野 (〒980-8574 仙台市青葉区星陵町 1-1)
Corresponding author : Atsuhiro NAKAGAWA, M.D., Department of Neurosurgery, Tohoku University Graduate School of Medicine, 1-1 Seiryo-machi, Aoba-ku, Sendai-shi, Miyagi 980-8574, JAPAN

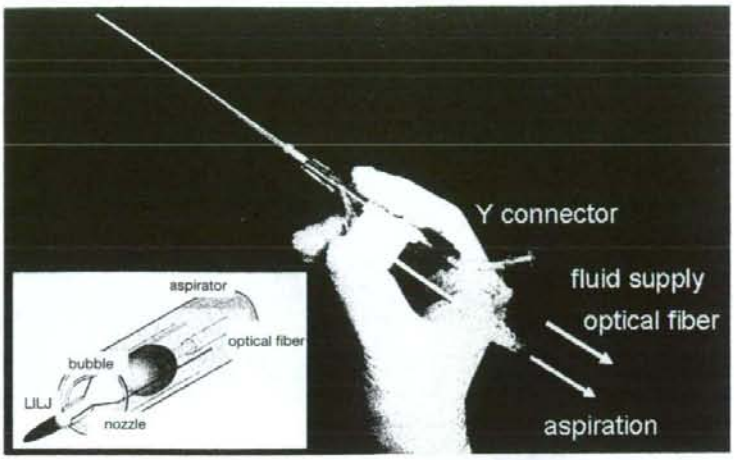

Fig. 1 Overview of the LILJ system. LILJ was generated by irradiating pulsed Ho: YAG laser within a stainless tube, filled with cold (4℃) lactated Ringer's solution. The laser was conducted through optical quartz fiber. Transient expansion of laser-induced bubble pushes the liquid distal to the tip of the optical fiber. The jet generated was ejected from a stainless nozzle. To avoid splash and air bubbles within the surgical field, the nozzle was placed inside a stainless suction tube.

I. はじめに

液体（水）ジェットメスは水流により組織を線状に切開，もしくは体積をもつ塊として破砕するデバイスである．最大の特徴は熱損傷がない点と高い組織選択性をもち細血管（200 μm 程度）温存下に組織切開・破砕が可能である点である[21,26]．こうした特性は早くから注目され，25 年以上前から腹部外科を中心に臨床応用されてきた[21]．特に，脳と同様に細血管からの出血や胆管損傷の処置に難渋する肝切除術では，既存の手術デバイス（超音波手術装置）と比較して手術時間短縮と出血量減少効果が報告されている[7]．その一方，従来の液体ジェットメスでは術野外に飛沫が飛散することによる播種や医療従事者への感染の危険性，術野内での気泡発生や水分貯留による視野悪化，微調整や小型化が困難といった問題から顕微鏡手術機器としては普及していないのが実情である．

工学的には，前述の問題点は高圧連続流の利用が少なからず関与しているものと考えられる[2]．パルスレーザージェットメスは，holmium：yttrium-aluminum-garnet（以下 Ho：YAG，ホルミウムヤグ）レーザーを駆動源として，実効水量が極めて微量の高速液体ジェットをパルス状に発生させ組織の切開・破砕を行うデバイスである．これまでの基礎実験では，効果ならびに安全性に関して従来の液体ジェットメスと同等以上であることを報告してきた[3-6,10,13-15,20,24]．2007 年 3 月に東北大学病院倫理委員会の承認を得て同年 5 月から臨床応用を開始し，これまでテント上神経膠腫 4 例において使用した経験を報告する．

II. 方　法

対象は 2007 年 5 ～ 7 月に東北大学病院で摘出術を施行したテント上神経膠腫 4 例である．パルスレーザージェットメスを用いて，切除予定脳内もしくは腫瘍内で径 2 mm 以下の動脈を含む領域内で液体ジェットを照射し，操作性と血管温存能力について評価を行った．

パルスレーザージェットメスは，液体ジェット発生部と吸引システムから構成される（**Fig. 1**）．液体ジェット発生部は吸引管（11 G ステンレス製，外径 3.06 mm，内径 2.64 mm）内腔に配置しており，液体ジェット射出管（18 G ステンレス製，

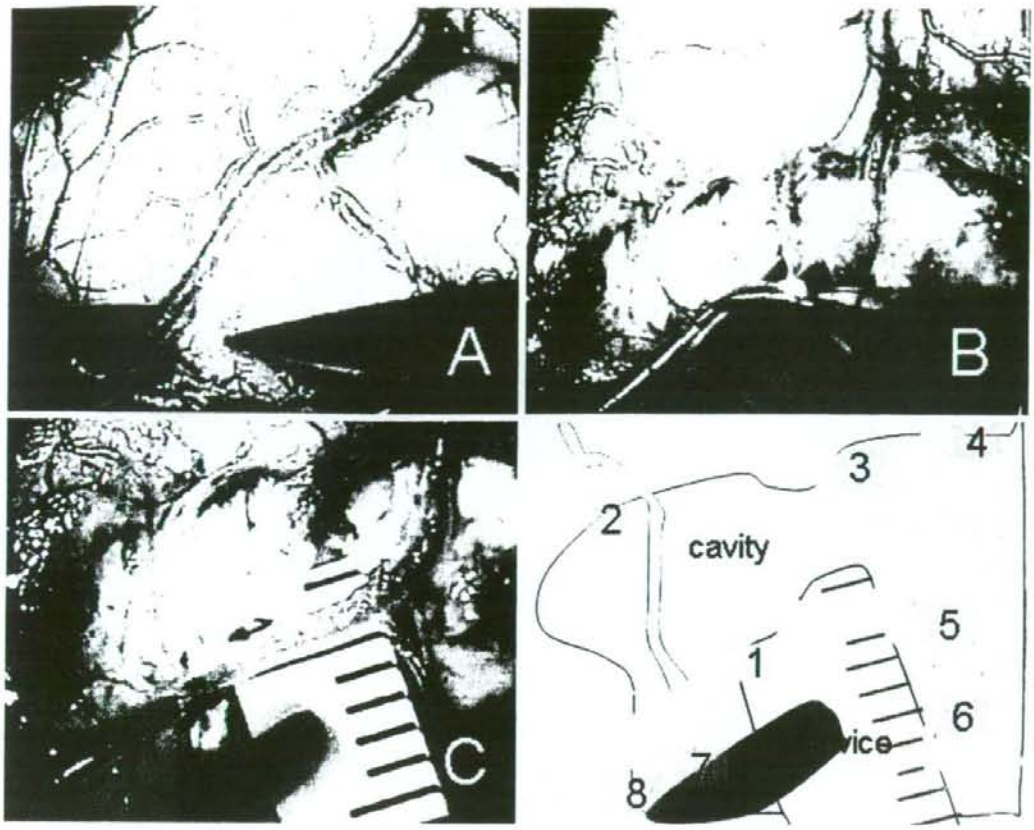

Fig. 2 Restoration of fine arteries after removal of brain tissue (diameter: 100 to 200 μm). Under the microscopic view, there was no significant occurrence of splash and air bubbles. **A**: Before removal. **B**: The arterial component is preserved even after direct ejection of LILJ toward a fine artery. **C**: After removal of brain tissue around the artery showing preservation of the fine arteries. **D**: Schematic diagram describing **C**, preservation of fine arteries in the removed cavity (1 to 8). Scale shows 1 mm. Smallest diameter of a preserved artery was 100 to 200 μm.

外径 1.26 mm，内径 0.90 mm），Y コネクター（アンプラスト®C Y コネクター AP-YC15S；テルモ㈱，東京），石英光ファイバー（無水石製，コア径 400 μm）で構成され，石英光ファイバーは Y コネクターにより液体ジェット射出管内に固定される．パルスレーザー光源は波長 2.1 μm の Ho：YAG レーザー（スパークリングフォトン㈱，東京；SLS-HO）で，レーザー光は石英光ファイバーにより液体ジェット発生部まで導光される．液体ジェット発生部には Y コネクターを介して 4℃に冷却された輸液（ラクテック®注；㈱大塚製薬工場，徳島）が供給され，管内部は常時満たされた状態となっている．液体ジェット射出管内にレーザー光がパルス照射されると一過性に蒸気泡が発生・膨張し，気泡の前方にある液体がノズル（19 G ステンレス製，外径 1.06 mm，内径 0.70 mm）方向へ押し出され，パルス状の液体ジェットが射出される．

液体ジェットによる組織深達度は液体ジェットの噴出圧，初速に比例し，レーザーエネルギー，standoff distance（光ファイバー出射端とノズル先端間距離），ノズル（アスペクト）比による調節が可能であるが[3-6,10,13-15,20,24]，今回の検討では，簡便性の点からレーザーエネルギーによる調節を行い（233 ～ 300 mJ/pulse），standoff distance は 10 cm で固定した．吸引システムは通常の手術吸

引装置に接続して使用した．操作は超音波手術装置と同じ要領で，レーザーのフットスイッチを踏み込むとパルス液体ジェットがノズルから射出され，飛沫，余剰水分，破砕片は吸引管から回収されるようになっている．

III. 結　果

液体ジェットが線維成分に富むくも膜は貫通しないことは，ブタを用いた詳細な検討で報告されているが[16]，今回の検討でも同様で膜成分を超えて深達することはなく，マイクロ鑷子にて別に剝離した．今回使用したエネルギーの範囲内では，低エネルギーでは連続照射により神経膠腫・正常脳組織を線状に切開することが可能で，エネルギーの増加に伴い組織を一塊として破砕することも可能であった．動脈に関しては径100～200 μm程度の血管までの温存が可能であったが，同径の静脈温存効果は認められなかった．操作性に関しては顕微鏡視野で問題となるような飛沫，気泡の発生は認められず，パルスレーザージェットメスの使用による合併症は認められなかった．これまでのところいずれの症例においても播種は認められていない．

症例呈示

〈症　例〉 65歳　女性

診　断　右側頭葉～島部神経膠芽腫

手術操作　通常の右前頭側頭開頭を行った．顕微鏡下操作に入り，深部の腫瘍摘出に先立ち右側頭葉部分切除を行う際にパルスレーザージェットメスを使用した．切除予定脳表領域内部で径1 mm程度の動脈を含む2×3 cm，深さ1 cm程度の領域(**Fig. 2A**)の切開・破砕をレーザージェットメスで行った．液体ジェットはくも膜は貫通しなかったため，マイクロ鑷子を用いて脳表血管のくも膜を剝離した．その後，径1 mm程度の動脈と脳実質を一塊として液体ジェットを照射したところ，脳実質のみこそげ落ちるように破砕されたが，動脈は温存された(**Fig. 2B**)．続いて分枝している動脈と脳実質を一塊として照射した．今回のデバイスでは吸引の微調整が十分ではなく，吸引管径が大きいために吸引管による視野が妨げられ，いったん温存した後に吸引管で損傷する場面もあった．その一方で，特に血管の走行を意識することなく液体ジェットを射出したにもかかわらず，径100～200 μm程度の分枝までは温存された(**Fig. 2C, D**)．また，顕微鏡操作に支障を来す飛沫や気泡の発生は認められず，血管の間隙や血管の深部での破砕操作も可能であった．温存された動脈と同径の細静脈は液体ジェットによる物理的損傷により温存は困難であった．

IV. 考　察

神経膠腫摘出術では，病変の摘出率向上と術後神経学的後遺症を出さないこととの両立が求められる[1,9]．1990年代以降，脳機能マッピング，ニューロナビゲーションシステムなどの導入により摘出術の際の機能温存方法に関しては格段に進歩した．しかし神経膠腫摘出術中の穿通枝の温存については克服すべき課題が多い．例えば島部神経膠腫，前頭弁蓋部腫瘍摘出術における外側線条体動脈，髄質動脈は血管径が1 mm以下と非常に細いにもかかわらず，損傷が重篤な麻痺につながることが報告されている[11,12]．

これまで，腫瘍摘出術に際しては電気，超音波，レーザー，電磁式手術デバイスなどを適宜組み合わせ行っているが，調節性，操作性に関しては優れている反面，熱損傷の防止と細血管の温存に関しては限界がある．このため，液体ジェットメスは以前より従来の手術デバイスの短所を補い得るものとして期待されてきた(**Table**)．近年，高圧連続流を用いるタイプの液体ジェットメスも改良され，欧州の一部脳神経外科施設で臨床応用されており[8,16-19,22,23,25,27]，熱損傷がなく細血管が温存されること，超音波手術装置との比較を行ったところ，手術時間の延長はなく，出血量減少効果があったとされている[22,23]．その一方で，前述した高圧連続流の使用による諸問題の解消には限界があり，既存の手術デバイスとの比較において際立った優位性を打ち出せず，普及していないのが実情である．今回高速パルス液体ジェットを用いた結果，第一に微調整が可能で穿通枝レベルの血管